CHEMISTRY OF MATERIALS
Cite This: Chem. Mater. 2018, 30, 1011−1016
Article
pubs.acs.org/cm

Gate Tunable Self-Biased Diode Based on Few Layered MoS_2 and WSe_2

Muhammad Atif Khan,[†] Servin Rathi,[†] Dongsuk Lim,[†] Sun Jin Yun,[§] Doo-Hyeb Youn,[§] Kenji Watanabe,[¶] Takashi Taniguchi,[¶] and Gil-Ho Kim*[,†]

[†]School of Electronic and Electrical Engineering and Sungkyunkwan Advanced Institute of Nanotechnology (SAINT), Sungkyunkwan University, Suwon 16419, South Korea

[§]ICT Components and Materials Technology Research Division, Electronics and Telecommunications Research Institute, Daejeon 34129, South Korea

[¶]National Institute for Materials Science, Namiki, Tsukuba, Ibaraki 305-0044, Japan

Supporting Information

ABSTRACT: The operation of a self-biased diode (SBD) based on MoS_2 has been demonstrated by using an asymmetric top gate comprising metal-hexagonal boron nitride (h-BN)-MoS_2 structure. The rectification is achieved by asymmetric modulation of effective Schottky barrier and carrier density in the channel during forward and reverse bias, and a rectification factor of 1.3×10^5 is achieved in $I-V$ characteristics. The modulation of effective Schottky barrier is verified by temperature dependent measurement in a range of 173 to 373 K, and a difference of 300 meV is observed in effective Schottky barrier height for forward and reverse bias. The electrical characteristics of SBD exhibit close resemblance with an ideal thermionic emission model with an ideality factor of 1.3. SBD also exhibits strong photoelectrical response with a specific detectivity of 150 A/W and responsivity of 2.1×10^{10} Jones under 450 nm laser light illumination. In the end, to demonstrate the diversity of the proposed scheme, SBD based on WSe_2 has also been fabricated and the results have been discussed. These results suggest a new route toward the SBD based numerous electronics and optoelectronics applications and can in principle be implemented using other two-dimensional materials as well.

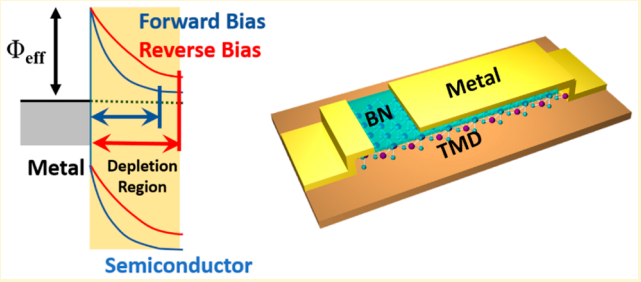

1. INTRODUCTION

Diode is a vital circuit component with the key feature of extremely asymmetric current−voltage characteristics for forward and reverse bias. The importance of the diode is well-known as numerous analog and digital circuits can be realized using diodes.[1] In conventional design of bulk semiconductor, the diode is usually fabricated by controlled doping of semiconductor and forming a p−n junction between two regions of the semiconductor. This process utilizes conventional doping techniques like diffusion doping and ion implantation.[1] However, at the nanoscale, when the active channel size is extremely small, these conventional doping techniques have severe limitations. The number of dopant atoms at the nanoscale becomes less than 100, thus posing a serious challenge to realize stable and controllable doping.[2,3] Therefore, conventional doping techniques are no longer effective to realize a diode at the nanoscale, and other schemes should be used to modulate and control the semiconductor properties.

Two-dimensional (2D) materials have strong potential to replace conventional bulk semiconductor materials for sub-5 nm electronics because of several unique properties like atomic scale thickness, sizable band gap, and high mobility.[4−7] Diode is a solicitous device in the field of 2D materials based electronics as well, and therefore, several new schemes for diodes have been proposed based on these 2D materials. These schemes include p−n junction fabricated by heterostructure of MoS_2 and WSe_2,[8] split gate induced p−n junction in WSe_2,[9] and freezing ion technique in ion gel at low temperature to form a p−n junction.[10] Some new surface doping techniques like p-doping in MoS_2 by $AuCl_3$ solution[11] and plasma assisted doping[12] to fabricate p−n junction in MoS_2 have also been proposed to form a p−n junction in a single flake. Besides the typical p−n junction diode, the Schottky diode where the modulation of depletion width at the metal−semiconductor interface results in rectifying behavior has also been studied. These diodes by the virtue of their fast switching time and low power consumption are commonly used in high speed digital circuits and analog amplifiers. In 2D materials, rectifying characteristics similar to those of Schottky diodes have been achieved by using a thin dielectric layer as the tunneling barrier for one of the contact electrodes.[13,14] Further, contact

Received: November 20, 2017
Revised: December 29, 2017
Published: January 4, 2018

DOI: 10.1021/acs.chemmater.7b04865
Chem. Mater. 2018, 30, 1011−1016

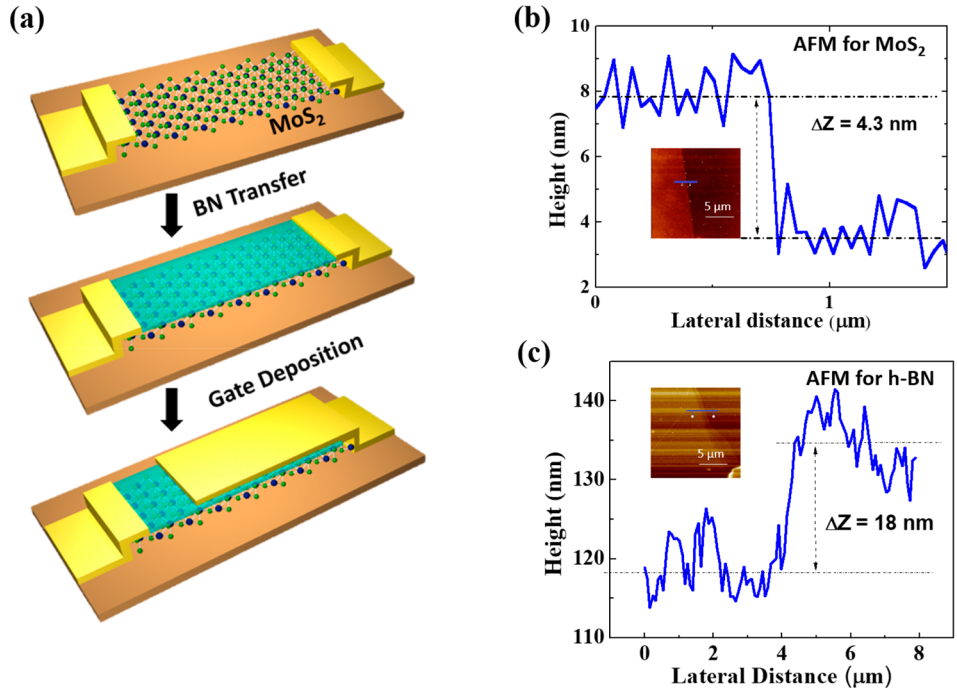

Figure 1. (a) Schematic drawing of the SBD illustrating the fabrication steps. (b and c) Atomic force microscopy (AFM) image of (b) MoS_2 with the height profile and (c) h-BN with the height profile.

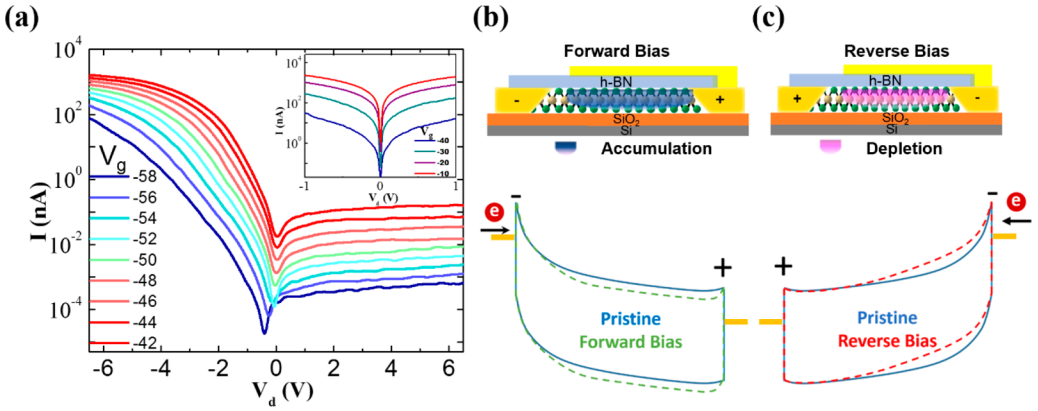

Figure 2. (a) Output characteristics of SBD at different back gate voltage in semilogarithmic scale (inset shows output characteristics of device before deposition of top electrode in semilogarithmic scale). (b and c) Schematic illustrating (b) accumulation of electrons in MoS_2 SBD under forward bias and corresponding schematic band diagram and (c) depletion of electrons in MoS_2 SBD under reverse bias and corresponding schematic band diagram.

resistance is also one of the major issues in the realization of 2D material based electronics and is mainly due to the absence of suitable techniques to address the formation of a Schottky barrier at the metal−2D material interface.[15] However, modulating this Schottky barrier at the metal−semiconductor during forward and reverse bias can lead to the appearance of the rectifying $I-V$ curve, which could be used as the scheme to design high performance diodes based on 2D materials.

In this work, we have demonstrated the operation of a self-biased diode (SBD) by using an asymmetric top gate and modulating the carrier density in the channel and Schottky barrier at the metal MoS_2 interface during forward and reverse bias. A high asymmetry of around 10^5 is achieved in $I-V$ output characteristics, which is attributed to asymmetric modulation of the Schottky barrier during forward and reverse bias. This scheme can be implemented using other 2D materials as well, and as an example, operation of SBD based on WSe_2 has also been demonstrated. These results suggest a new route toward the SBD based device applications.

Figure 1a is the schematic drawing of the SBD showing the steps of device fabrication. In the first step, MoS_2 is exfoliated on the Si/SiO_2 substrate and suitable flakes are selected by optical microscope. The pattern of electrodes is formed by photolithography which is followed by metal deposition (Cr/Au). Using the dry transfer technique, few layered h-BN is transferred on the device. In the end, top gate metal is deposited using e-beam lithography followed by metal deposition in such a way that the top gate is connected to one of the electrodes as well. Raman spectroscopy is used to characterize the flakes and is shown in Figure S1. The Raman spectrum, which was taken at room temperature using a 532 nm laser, shows signature peaks E_{2g}^1 and A_{1g} of MoS_2 confirming the flake as MoS_2. The thickness of MoS_2 and h-BN is determined by AFM and is shown in Figure 1b,c,

DOI: 10.1021/acs.chemmater.7b04865
Chem. Mater. 2018, 30, 1011−1016

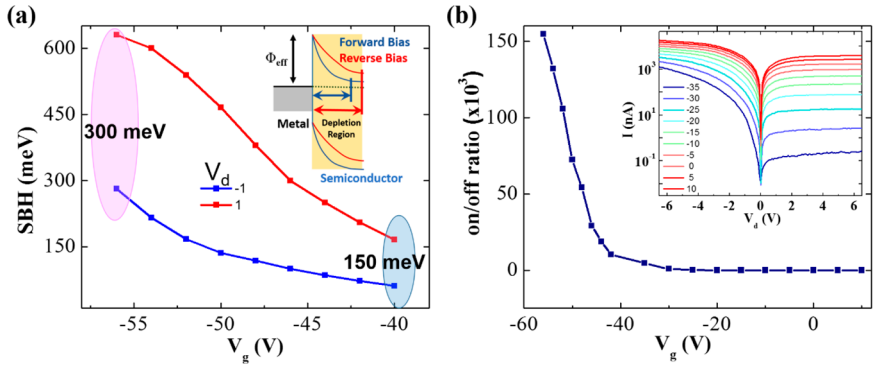

Figure 3. (a) Variation in effective Schottky barrier height with back gate voltage during forward and reverse bias. (b) Plot between on/off ratio of SBD and back gate voltage (inset shows output characteristics of SBD at high back gate voltage in semilogarithmic scale).

respectively. MoS_2 thickness is around 4.3 nm (6 layers), whereas h-BN thickness is around 18 nm.

2. RESULTS AND DISCUSSION

Figure 2a illustrates the output characteristics of the SBD. The inset of Figure 2a shows output characteristics of the device before deposition of the top electrode, and it can be seen that the $I-V$ curve is symmetric, which indicates the presence of Ohmic-like contacts. However, after deposition of the top electrode, the $I-V$ curve becomes highly asymmetric with the rectification ratio of around 10^5 when the applied voltage is changed from −6.5 to 6.5 V. This asymmetric transport behavior is a typical feature of the rectifying diode. The output characteristics are obtained for different back gate voltages, and it is observed that although the current for positive as well as negative applied drain changes with the gate voltage, the rectification ratio remains almost unchanged for all the gate voltages from −58 V to −42 V. The mechanism behind this highly asymmetric transport has been explained by schematics in Figure 2b,c. When a negative voltage is applied to the left electrode and the extended right electrode is positive, the SBD is in forward bias. The extended electrode also acts as the top gate and thus can affect both carrier concentration in the underlying channel and the effective Schottky barrier height (SBH) at the extended electrode junction. According to the Schottky−Mott rule, SBH is a function of the difference between the metal work function and the electron affinity of the semiconductor. However, at a metal−semiconductor junction, besides conventional thermionic emission across the barrier, the total carrier injection includes thermionic field emission and a tunneling component as well. While the former component is fixed for a particular metal and semiconductor junction, the latter depends upon the depletion width which can be modulated by several methods like electrostatic gating, doping, etc. Therefore, even for a fixed SBH, total carrier injection can vary depending upon depletion width and hence give the impression of a variable SBH known as effective SBH. The main aim of incorporating the extended electrode in the device layout is to utilize the modulation of this effective SBH to control the device characteristics.

During forward bias, by virtue of the positive electric field from the extended top electrode, electrons are accumulated in the MoS_2 channel as shown in Figure 2b. This makes the channel highly conductive, and significantly high current flows through the MoS_2 channel. Moreover, as shown in the schematic band diagram, during forward bias (green line), the Schottky barrier at the left metal electrode−MoS_2 interface remains unaffected. This is because the injection of electrons in the MoS_2 channel is from the negative electrode (left electrode in forward bias), which is not in the vicinity of the extended top electrode; therefore, the Schottky barrier remains unchanged at this junction and significantly high current flows through the device by the virtue of high conducting channel under the extended electrode. During reverse bias, the left electrode is positive while the extended electrode is negative as shown in Figure 2c. As the extended electrode is also an injection point now, the current is therefore affected by both variations in carrier concentration and effective SBH at this electrode. The negative electric field from the extended electrode depletes the electrons in the MoS_2 channel, thus making the channel resistive and resulting in significantly reduced current flow in the MoS_2 channel. Moreover, unlike forward bias, during reverse bias the value of the effective Schottky barrier at the metal−MoS_2 interface is increased from its pristine state due to depletion of electrons in the MoS_2 channel. As the majority of the electrons are injected in the channel via thermionic field assisted quantum mechanical tunneling through the barrier, the increase in the effective Schottky barrier height will reduce the electron injection. Therefore, along with high channel resistance, carriers will also experience increased effective SBH during reverse bias which ultimately leads to decrease in the device current.

To verify this explanation of modulation of effective Schottky barrier with applied bias, we performed the temperature dependent measurement of our SBD. The output characteristics of the SBD are measured at different gate voltages in a temperature range of 173 to 373 K (step size: 20 K). Equation 1 can be used to describe the carrier transport at a Schottky metal−MoS_2 contact.[16,17]

$$I = AA^*T^{3/2}\exp\left(-\frac{e\varnothing_b}{k_BT}\right)\left(\exp\left(\frac{eV_d}{k_BT}-1\right)\right) \quad (1)$$

In this equation, I is the current, A is the device area, A^* is the modified Richardson constant, $\varnothing_b$ is the Schottky barrier height, V_d is the applied drain voltage, e is the electron charge, k_B is Boltzmann constant, and T is temperature in Kelvin. This equation assumes that the application of a high drain voltage (V_d) reduces the influence of the Schottky barrier at the drain to negligible levels and the current flow is dominated by the Schottky barrier at the source side only.[16,17] Under this assumption, we measured the current as a function of the temperature and extracted the effective SBH from the slope of linear fit to $\ln(I/T^{3/2})$ as a function of $1/T$ at different back gate

DOI: 10.1021/acs.chemmater.7b04865
Chem. Mater. 2018, 30, 1011−1016

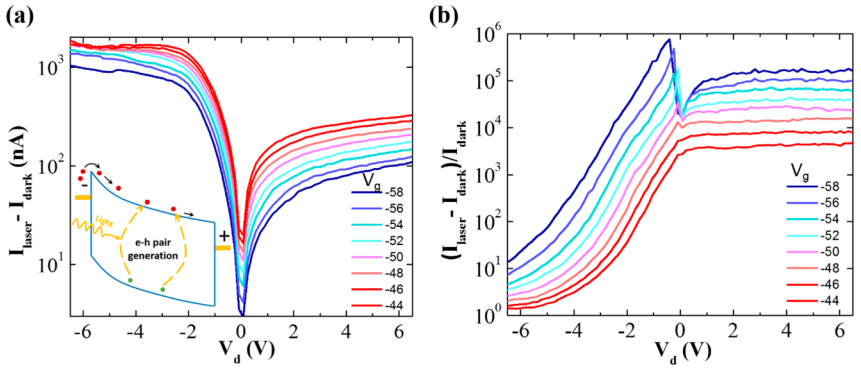

Figure 4. (a) Photocurrent characteristics of SBD obtained by subtracting dark current from total laser current at different back gate voltages in semilogarithmic scale. (b) Relative variation in photocurrent at different drain voltages of SBD.

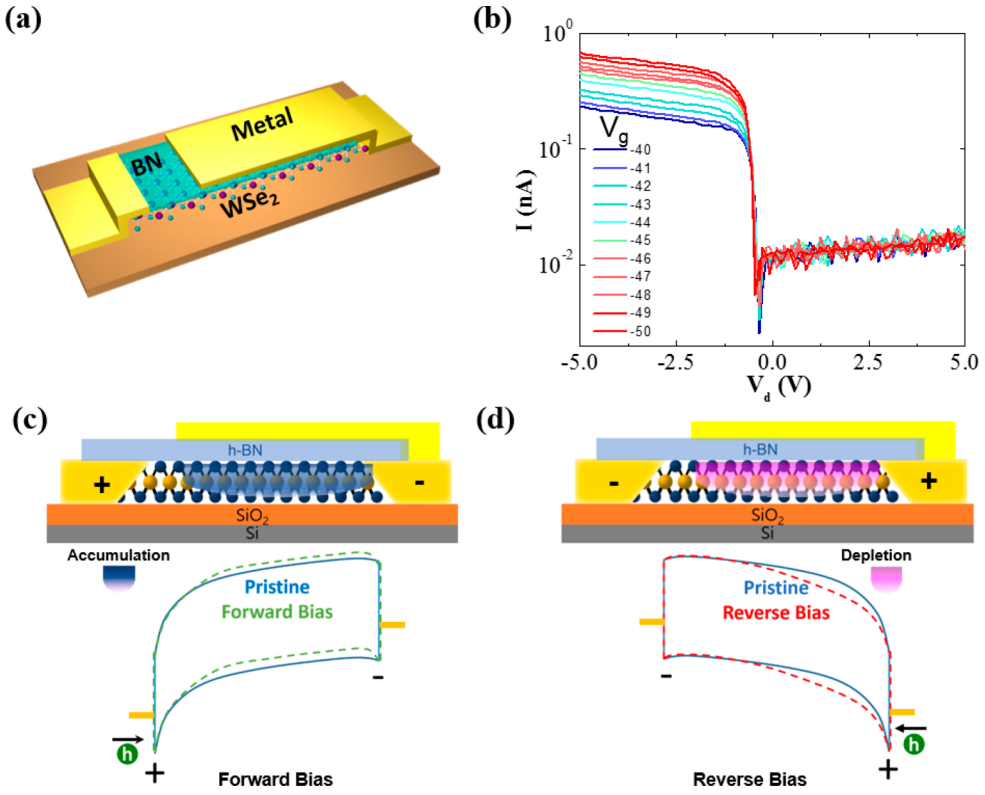

Figure 5. (a) Schematic of WSe_2 based SBD. (b) Output characteristics of WSe_2 based SBD. (c and d). Schematic and corresponding band diagram showing (c) accumulation of holes during forward bias and (d) depletion of holes during reverse bias.

voltages. The slope of a linear fit yielded the effective SBH for different V_g, as shown in Figure 3a.

Figure 3a shows the extracted value of the effective Schottky barrier for different gate voltages during forward bias as well as reverse bias. There are two major observations in Figure 3a: first, at the same V_g, SBH for reverse bias is more than twice that of the forward bias. For example, at $V_g = -56$ V, SBH is around 300 meV for forward bias and 620 meV for reverse bias. This observation of the difference in SBH verifies the earlier explanation where the observed diode behavior is attributed to asymmetric effect of the extended electrode on the modulation of the effective SBH so that carriers experience different effective SBH during forward and reverse bias (Figure 2b,c). Second, it can be seen that the value of SBH substantially depends on V_g as well. For both forward and reverse bias, increase in V_g results in the increase in carrier concentration in the channel which leads to the reduction in the effective SBH at metal−MoS_2 junctions. However, the rate of variation in the SBH with V_g is not the same for forward and reverse bias and hence the difference between SBH for forward bias and reverse bias also changes with V_g. For example, at $V_g = -56$ V, the difference in SBH for forward bias and reverse bias is around 300 meV, which is reduced to around 150 meV at $V_g = -40$ V. The explanation for this behavior is that, by increasing V_g, the carrier concentration in the channel increases and therefore the influence of depletion induced by the top electrode on the modulation of SBH becomes less effective. This converging trend in the difference of SBH for forward and reverse bias is also reflected in the electrical characteristics where on/off ratio of SBD decreases with V_g (Figure 3b), and as seen in inset of Figure 3b the $I-V$ curve becomes almost symmetrical for $V_g = 10$ V. This unique feature to dynamically modulate the on/off

DOI: 10.1021/acs.chemmater.7b04865
Chem. Mater. 2018, 30, 1011−1016

ratio in the semiconducting diode can be an advantage of the proposed technique where the on/off ratio of SBD can be modulated and the desired value of on as well as off current can be achieved by changing V_g.

Photodevices including LEDs and solar cells also constitute an important application of diodes. The photoresponse of SBD at different V_g under illumination of monochromatic light of wavelength 450 nm is shown in Figure 4. The opto-electrical response of SBD exhibits the feature of a typical diode. The illumination of the device with the laser resulted in a minor increase in the on-current, whereas in the off-region, a large increase in the device current was observed, which is attributed to photogenerated electron−hole pairs as shown in the inset of Figure 4a. We have also evaluated the performance of our SBD by calculating responsivity and specific detectivity of the device. Responsivity is the ratio of photo current to incident optical power, $R = I_{ph}/P_{in}$, where I_{ph} is obtained by subtracting I_{dark} from the total current under illumination I_{laser}. Specific detectivity (D^*) is calculated by $D^* = A^{1/2}/NEP$, where A is the illuminated area and NEP is the noise equivalent power, NEP = $(2qI)^{1/2}/R$.[11,14,18] Specific detectivity enables the comparison of the device with different geometries, and it is a measure of detector sensitivity. The maximum obtained value of responsivity is 150 A/W at $V_d = -6.5$ V, while the maximum value of detectivity is 2.1×10^{10} Jones. These values are comparable to previous published data on TMD-based photodetectors and manifest the advantage of SBD to be used in photodetector applications.[11,14,18]

Next, we have calculated the ideality factor for our SBD which is a parameter generally used to measure the deviation of practical diodes from the ideal thermionic emission model. We have used the following equation for the Schottky barrier diode with series resistance to calculate the ideality factor.[19,20]

$$\frac{dV_d}{dL_nI} = n\frac{kT}{q} + IR_s \quad (2)$$

where V_d is the applied voltage, I is the device current, n is ideality factor, k is Boltzman's constant, T is temperature in Kelvin, q is electron charge, and R_s is series resistance. The Experimental plot of $\frac{dV_d}{dL_nI}$ vs I of SBD at room temperature is presented in Figure S3. After fitting the curve to a straight line and using eq 2, the value of n is determined from the graph, which comes out to be $n = 1.3$. The value of 1.3 indicates that transport behavior of our SBD exhibits close resemblance with the ideal thermionic emission model. The observed deviation from the ideal diode behavior could be due to nonidealities like process chemical residues, material defects, and traps at the metal−MoS_2 interface which could lead to recombination at the junction thus resulting in the higher value of the ideality factor.

Further to demonstrate the diversity of the proposed SBD configuration, we fabricated the SBD based on WSe_2 as shown in Figure 5a. Figure 5b presents the output characteristics of WSe_2 based SBD. Like MoS_2 SBD, WSe_2 SBD also exhibits asymmetry in the output curve. A rectification factor of around 10^2 is achieved, which is attributed to modulation of the Schottky barrier as well as accumulation and depletion induced by the top electrode during forward bias and reverse bias, respectively. However, as shown in Figure 5c,d, the operation of WSe_2 based SBD is quite different from that of MoS_2 based SBD. In MoS_2, the majority carriers are electrons whereas WSe_2 is a p-type material where holes are majority carriers.[21,22] In WSe_2 based SBD, during forward bias, the extended electrode is negative, whereas the left electrode is positive. The extended electrode will generate negative electric field to accumulate holes in the WSe_2 channel, thus making the channel conductive as shown in Figure 5c. This accumulation of holes will result in high device current during forward bias. During reverse bias, the left electrode is negative while the extended electrode is positive as shown in Figure 5d. The extended electrode will generate positive electric field to deplete holes in the channel, thus making the channel more resistive. Moreover, during reverse bias, the extended electrode serves as the source; thus, depletion at this electrode will result in increased SBH resulting in reduced current flows through the device. The on/off ratio in WSe_2 SBD is around 10^2 which is much less than the on/off ratio of MoS_2 SBD. This difference in the on/off ratio can be attributed to multiple factors like WSe_2 thickness, h-BN thickness, contact resistance, and Schottky barrier height at the metal−WSe_2 interface.

3. CONCLUSION

The operation of SBD based on MoS_2 has been demonstrated. A high rectification factor of 1.3×10^5 is achieved in $I-V$ output characteristics. This rectification factor can be modulated by back gate, and the desired level of output current can be achieved. The asymmetry in the $I-V$ curve is due to modulation of the Schottky barrier in the channel during forward and reverse bias as verified by temperature dependent measurement, and a difference of 300 meV is observed in the Schottky barrier height for forward and reverse bias. SBD exhibits specific detectivity of 150 A/W and responsivity of 2.1×10^{10} when illuminated by monochromatic light of 450 nm. In the end, SBD based on WSe_2 has been fabricated, which also demonstrated rectifying characteristics. These results suggest a new route toward the SBD based devices for numerous electronic and optoelectronic applications.

4. EXPERIMENTAL METHODS

The MoS_2 flakes were produced by standard mechanical exfoliation using the scotch tape technique from a commercial bulk MoS_2. The flakes were exfoliated on a silicon substrate with 285 nm SiO_2. Suitable flakes were selected using an optical microscope, the thickness of these flakes was identified with AFM, and Raman spectroscopy was used to characterize the flakes. The back-gated SBDs were fabricated by photolithography to define electrical contacts on selected flakes followed by Cr/Au (10/30 nm) deposition and lift off in acetone. Using the same method, h-BN flakes were exfoliated and selected. h-BN flakes were transferred on top of the MoS_2 device by a dry transfer technique.[23] After h-BN transfer, the top gate electrode is defined by e-beam lithography followed by Cr/Au deposition and lift off in acetone.

■ ASSOCIATED CONTENT

Supporting Information

The Supporting Information is available free of charge on the ACS Publications website at DOI: 10.1021/acs.chemmater.7b04865.

Raman spectrum and optical microscope image of MoS_2 and WSe_2 SBD, $I-V$ characteristics of MoS_2 based SBD before the deposition of extended top electrode, dV/dL_nI vs I plot of MoS_2 SBD, plot of MoS_2 SBD total current under laser illumination (I_{laser}) vs V_d, output characteristics of SBD in linear scale, and Shockley diode equation based model of SBD (PDF)

DOI: 10.1021/acs.chemmater.7b04865
Chem. Mater. 2018, 30, 1011−1016

AUTHOR INFORMATION

Corresponding Author

*(G.-H.K.) Tel.: +82-31-290-7970. E-mail: ghkim@skku.edu.

ORCID

Sun Jin Yun: 0000-0002-3665-0393
Kenji Watanabe: 0000-0003-3701-8119
Gil-Ho Kim: 0000-0003-2479-5357

Notes

The authors declare no competing financial interest.

ACKNOWLEDGMENTS

This research was supported by Basic Science Research Program through the National Research Foundation of Korea (NRF) funded by the Ministry of Education, Science and Technology, 2016R1A2A2A05921925 and 2016R1D1A1B03932455, and Korea Research Fellowship Program through the NRF funded by the Ministry of Science and ICT (2015H1D3A1062519). This work was partly supported by Institute for Information & Communications Technology Promotion grant funded by the Korean government (B0117-16-1003, Fundamental technologies of two-dimensional materials and devices for the platform of new-functional smart devices). Growth of hexagonal boron nitride crystals was supported by the Elemental Strategy Initiative conducted by the MEXT, Japan, and JSPS KAKENHI Grant Numbers JP15K21722 and JP25106006.

REFERENCES

(1) Sze, S. *Physics of Semiconductor Devices*. John Wiley and Sons, New York 1981.

(2) Bernstein, K.; Frank, D. J.; Gattiker, A. E.; Haensch, W.; Ji, B. L.; Nassif, S. R.; Nowak, E. J.; Pearson, D. J.; Rohrer, N. J. High-performance CMOS Variability in the 65-nm Regime and Beyond. *IBM J. Res. Dev.* **2006**, *50* (4.5), 433−449.

(3) Asenov, A.; Brown, A. R.; Davies, J. H.; Kaya, S.; Slavcheva, G. Simulation of Intrinsic Parameter Fluctuations in Decananometer and Nanometer-Scale MOSFETs. *IEEE Trans. Electron Devices* **2003**, *50* (9), 1837−1852.

(4) Geim, A. K.; Novoselov, K. S. The Rise of Graphene. *Nat. Mater.* **2007**, *6* (3), 183−191.

(5) Wang, Q. H.; Kalantar-Zadeh, K.; Kis, A.; Coleman, J. N.; Strano, M. S. Electronics and Optoelectronics of Two-Dimensional Transition Metal Dichalcogenides. *Nat. Nanotechnol.* **2012**, *7* (11), 699−712.

(6) Xu, M.; Liang, T.; Shi, M.; Chen, H. Graphene-Like Two-Dimensional Materials. *Chem. Rev.* **2013**, *113* (5), 3766−3798.

(7) Chhowalla, M.; Shin, H. S.; Eda, G.; Li, L.-J.; Loh, K. P.; Zhang, H. The Chemistry of Two-Dimensional Layered Transition Metal Dichalcogenide Nanosheets. *Nat. Chem.* **2013**, *5* (4), 263−275.

(8) Lee, C.-H.; Lee, G.-H.; Van Der Zande, A. M.; Chen, W.; Li, Y.; Han, M.; Cui, X.; Arefe, G.; Nuckolls, C.; Heinz, T. F.; et al. Atomically Thin p−n Junctions with van der Waals Heterointerfaces. *Nat. Nanotechnol.* **2014**, *9* (9), 676−681.

(9) Ross, J. S.; Klement, P.; Jones, A. M.; Ghimire, N. J.; Yan, J.; Mandrus, D.; Taniguchi, T.; Watanabe, K.; Kitamura, K.; Yao, W.; et al. Electrically Tunable Excitonic Light-Emitting Diodes Based on Monolayer WSe_2 pn Junctions. *Nat. Nanotechnol.* **2014**, *9* (4), 268−272.

(10) Zhang, Y.; Ye, J.; Yomogida, Y.; Takenobu, T.; Iwasa, Y. Formation of a Stable p−n Junction in a Liquid-Gated MoS_2 Ambipolar Transistor. *Nano Lett.* **2013**, *13* (7), 3023−3028.

(11) Choi, M. S.; Qu, D.; Lee, D.; Liu, X.; Watanabe, K.; Taniguchi, T.; Yoo, W. J. Lateral MoS_2 p−n Junction Formed by Chemical Doping for Use in High-Performance Optoelectronics. *ACS Nano* **2014**, *8* (9), 9332−9340.

(12) Chen, M.; Nam, H.; Wi, S.; Ji, L.; Ren, X.; Bian, L.; Lu, S.; Liang, X. Stable Few-Layer MoS_2 Rectifying Diodes Formed by Plasma-Assisted Doping. *Appl. Phys. Lett.* **2013**, *103* (14), 142110.

(13) Chuang, S.; Battaglia, C.; Azcatl, A.; McDonnell, S.; Kang, J. S.; Yin, X.; Tosun, M.; Kapadia, R.; Fang, H.; Wallace, R. M.; Javey, A. MoS_2 p-type Transistors and Diodes Enabled by High Work Function MoOx Contacts. *Nano Lett.* **2014**, *14* (3), 1337−1342.

(14) Khan, M. A.; Rathi, S.; Lee, I.; Li, L.; Lim, D.; Kang, M.; Kim, G.-H. P-doping and Efficient Carrier Injection Induced by Graphene Oxide for High Performing WSe_2 Rectification Devices. *Appl. Phys. Lett.* **2016**, *108* (9), 093104.

(15) Allain, A.; Kang, J.; Banerjee, K.; Kis, A. Electrical Contacts to Two-Dimensional Semiconductors. *Nat. Mater.* **2015**, *14* (12), 1195−1205.

(16) Ahmed, F.; Choi, M. S.; Liu, X.; Yoo, W. J. Carrier Transport at the Metal−MoS_2 Interface. *Nanoscale* **2015**, *7* (20), 9222−9228.

(17) Kim, C.; Moon, I.; Lee, D.; Choi, M. S.; Ahmed, F.; Nam, S.; Cho, Y.; Shin, H.-J.; Park, S.; Yoo, W. J. Fermi Level Pinning at Electrical Metal Contacts of Monolayer Molybdenum Dichalcogenides. *ACS Nano* **2017**, *11* (2), 1588−1596.

(18) Rathi, S.; Lee, I.; Lim, D.; Wang, J.; Ochiai, Y.; Aoki, N.; Watanabe, K.; Taniguchi, T.; Lee, G.-H.; Yu, Y.-J.; et al. Tunable Electrical and Optical Characteristics in Monolayer Graphene and Few-Layer MoS_2 Heterostructure Devices. *Nano Lett.* **2015**, *15* (8), 5017−5024.

(19) Cheung, S.; Cheung, N. Extraction of Schottky Diode Parameters from Forward Current-Voltage Characteristics. *Appl. Phys. Lett.* **1986**, *49* (2), 85−87.

(20) Gholami, S.; Khakbaz, M. Measurement of IV Characteristics of a PtSi/p-Si Schottky Barrier Diode at Low Temperatures. *Int. J. Electr., Comput., Energ., Electron. Commun. Eng.* **2011**, *5* (9), 1285−1288.

(21) Lee, I.; Rathi, S.; Li, L.; Lim, D.; Khan, M. A.; Kannan, E.; Kim, G.-H. Non-Degenerate n-type Doping by Hydrazine Treatment in Metal Work Function Engineered WSe_2 Field-Effect Transistor. *Nanotechnology* **2015**, *26* (45), 455203.

(22) Fang, H.; Chuang, S.; Chang, T. C.; Takei, K.; Takahashi, T.; Javey, A. High-Performance Single Layered WSe_2 p-FETs with Chemically Doped Contacts. *Nano Lett.* **2012**, *12* (7), 3788−3792.

(23) Pizzocchero, F.; Gammelgaard, L.; Jessen, B. S.; Caridad, J. M.; Wang, L.; Hone, J.; Bøggild, P.; Booth, T. J. The Hot Pick-Up Technique for Batch Assembly of van der Waals Heterostructures. *Nat. Commun.* **2016**, *7*, 11894.

DOI: 10.1021/acs.chemmater.7b04865
Chem. Mater. 2018, 30, 1011−1016